Air Quality, Atmosphere & Health (2018) 11:535–548
https://doi.org/10.1007/s11869-018-0558-4

Stratospheric ozone intrusions during the passage of cold fronts over central Chile

Rodrigo J. Seguel[1] · Carlos A. Mancilla[1] · Manuel A. Leiva G.[2]

Received: 26 November 2017 / Accepted: 26 February 2018 / Published online: 7 March 2018

Abstract

This study analyzes tropospheric column ozone variability in the southern hemisphere as a function of ozone transport from the stratosphere to the troposphere and photochemical formation. Geographically, the study area was located in the mid-latitudes in South America (33° S), to the west of the Andes mountain range, in an area highly susceptible to stratospheric intrusions. Monthly ozonesonde measurements were recorded in Colina to ascertain seasonal vertical ozone distribution from the surface to the stratosphere between September 2010 and May 2012. Vertical distribution of the tropospheric ozone was measured in Talagante for fronts crossing from west to east in central Chile, during two periods in September 2014 and March 2015. These periods were significantly different in terms of the stratospheric ozone annual cycle and height of the tropopause. Our results showed rapid increases of approximately 50% in the tropospheric column ozone at time intervals shorter than 1 week. At the surface level, unusually enhanced ozone levels up to 10 parts per billion volume (ppbv) were observed during nighttime. Additionally, stratosphere-troposphere exchange (STE) preferentially occurred in spring and winter, with higher contribution during spring when the tropospheric column ozone attained its maximum concentration. These results provide valuable information regarding tropospheric ozone, a major local and global climate pollutant, to decision makers. In addition, they provide the research community with experimental data from the southern hemisphere, which helps bridge knowledge gaps in a region that has been rarely studied by national and international scientific communities.

Keywords Ozonesonde · Ozone intrusion · Tropospheric column ozone · Stratosphere-troposphere exchange

Introduction

Ozone (O_3) plays a key role in atmospheric chemistry and the environment. In the stratosphere, ozone protects life on earth by removing practically all incident solar radiation with wavelengths shorter than 290 nm (National Research Council 1982). However, in the troposphere, ozone can act as an important greenhouse gas owing to its strong absorption bands at 9, 9.6, and 14.4 μm in the terrestrial infrared radiation (Monks et al. 2015; Neuman et al. 2012). Therefore, relatively small changes in the tropospheric ozone concentration can produce significant changes in the earth's radiation balance. At the ground level, ozone impairs human lung function (Lippmann 1991; McConnell et al. 2002; Bell et al. 2004; Liu and Peng 2018), impacts ecosystem productivity and crops yields (Van Dingenen et al. 2009), and damages materials (Lee et al. 1996).

The tropospheric ozone budget typically includes in situ photochemical production following the oxidation of volatile organic compounds (VOCs) in the presence of nitrogen oxides ($NO_x = NO + NO_2$) (Fiore et al. 2015; Alvim et al. 2017; Toro et al. 2013, 2014). Further, return of air from the stratosphere to the troposphere at extratropical latitudes through the Brewer-Dobson circulation (Schoeberl 2004) and perturbations of the mid-latitude stratosphere caused by breaking planetary waves transport significant amounts of ozone from the stratosphere to the troposphere (Cooper et al. 2004; Anet et al.

Electronic supplementary material The online version of this article (https://doi.org/10.1007/s11869-018-0558-4) contains supplementary material, which is available to authorized users.

✉ Rodrigo J. Seguel
roseguel@icloud.com

[1] Environmental Department, Trade & International Advisory SAGU, Los Canteros 8666, Parque Industrial de La Reina, 7880340 Santiago, Chile

[2] Centro de Ciencias Ambientales y Departamento de Química, Facultad de Ciencias, Universidad de Chile, P.O. Box 653, Santiago, Chile

2017). Ozone is principally removed from the troposphere by chemical loss and dry deposition. However, the rate of removal varies as the lifetime of ozone is in order of days in the convective boundary layer (CBL), but is estimated to be 1 or 2 months in the free troposphere (Stohl et al. 2000; Young et al. 2013).

Several mechanisms of stratosphere-to-troposphere transport (STT) have been documented in literature after Danielsen (1968) proved that tropopause folds lead to irreversible transport of stratospheric ozone-rich air into the troposphere including its deep troughs and cutoff-low systems (Price and Vaughan 1993). Cases of stratospheric contributions, as high as 40%, have been reported in literature (Roelofs and Lelieveld 1997). Furthermore, stratosphere-troposphere exchange to the tropospheric ozone is expected to increase during the coming decades as a consequence of global warming and stratospheric ozone recovery (Stevenson et al. 2006; Hegglin and Shepherd 2009) and will have important implications for air quality. Therefore, understanding the factors that elevate baseline ozone, including in situ chemical production and exchange with stratospheric air, is essential for developing effective control strategies and identifying potential impacts on human health, ecosystems, and climate.

Unfortunately, most long-term records of ozonesonde measurements, which provide detailed ozone profiles up to ~ 30 km, are restricted to the northern hemisphere (NH) (Staehelin et al. 2002). In the southern hemisphere, gaps exist in Asia, Africa, and South America, especially at mid-latitudes. In the tropics, significant contributions have been made by the southern hemisphere Additional Ozonesonde (SHADOZ) network, which aims to provide insight into tropical chemistry and dynamics (Thompson et al. 2012). Other noteworthy initiatives in the region are the ozonesonde observation program conducted on the Easter Island (27.9° S, 109.27° W) in Chile and the global GAW station located at Ushuaia (Argentina), the latter, aiming to record the influence of the south polar vortex over the high latitudes of the South American continent. Therefore, filling the southern hemisphere gaps in mid-latitudes is essential for improving the understanding of spatial and temporal variations of ozone, determining background ozone concentrations, as well as helping to validate remote sensing.

In central Chile, the surface ozone at non-attainment areas has declined over the last two decades as a consequence of regulatory policies (Schultz et al. 2017; Seguel et al. 2012, 2013). For instance, the annual number of daily 8 h maximum above 61 parts per billion volume (ppbv) decreased from 151 days in 1998 to 44 days in 2016 in the Santiago Metropolitan Region (Fig. S1). However, historical information concerning surface ozone at rural and pristine locations is lacking despite high numbers of urban monitoring stations. Similarly, long-term records of vertical ozone measurements are limited. Therefore, the objectives of this study are to (1) assess altitudinal and seasonal variations in ozone composition in a region rarely studied by national and international communities and (2) improve understanding of impact of the stratosphere-troposphere exchange (STE) on ozone concentration in the lower troposphere and near surface layer at the mid-latitudes in the southern hemisphere over an area of Chile, which is considered to be highly susceptible to stratospheric ozone intrusions.

To address this goal, we conducted several ozonesonde campaigns in central Chile from September 2010 to March 2015. We analyzed the results of ozonesonde campaigns conducted over 17 months in Santiago area, which provided the context for two specific episodes of stratospheric ozone intrusions impacting the troposphere, a frontal system that occurred in late winter and a cutoff low that occurred during early fall.

Methodology

Field study in Colina

To obtain seasonal vertical ozone distribution from the surface to the stratosphere, monthly ozonesonde measurements were conducted in Colina, a suburban town located north of Santiago. The ozonesondes were launched from Colina (33° 12′ 19″ S, 70° 41′ 03″ W, 584-m altitude) between September 2010 and May 2012 at 14:00, generally during clear skies (Fig. 1).

Colina is located downwind of Santiago Metropolitan Region that has nearly eight million inhabitants, and is considered as a non-attainment area for ozone. In the Santiago basin, anthropogenic emissions significantly affect the first few kilometers of the troposphere. The ozonesondes from Colina allowed characterization of the vertical ozone distribution for a complex terrain in central Chile and assisted in the effective design of measurement studies to determine the STE.

Field campaign at Talagante

Talagante (33° 40′ 25″ S, 70° 57′ 11″ W, 341-m altitude), a suburban town located nearly 35 km southwest of Santiago (Fig. 1), offered several advantages for launching ozonesondes. Surface measurements exhibited low ozone mixing ratios; the annual average between 2010 and 2014 varied from 14 to 17 ppbv, and mean diurnal cycle during the period did not exceed 36 ppbv. In addition, the prevailing southwest winds facilitated fresh air inflow to the Santiago basin.

In September 2014 and March 2015, two ozonesonde studies were conducted in Talagante to observe STE during two typical winter and autumn weather events. These events corresponded to a frontal system and cutoff low, respectively. Both episodes lasted for 5 days and resulted in significant rainfall.

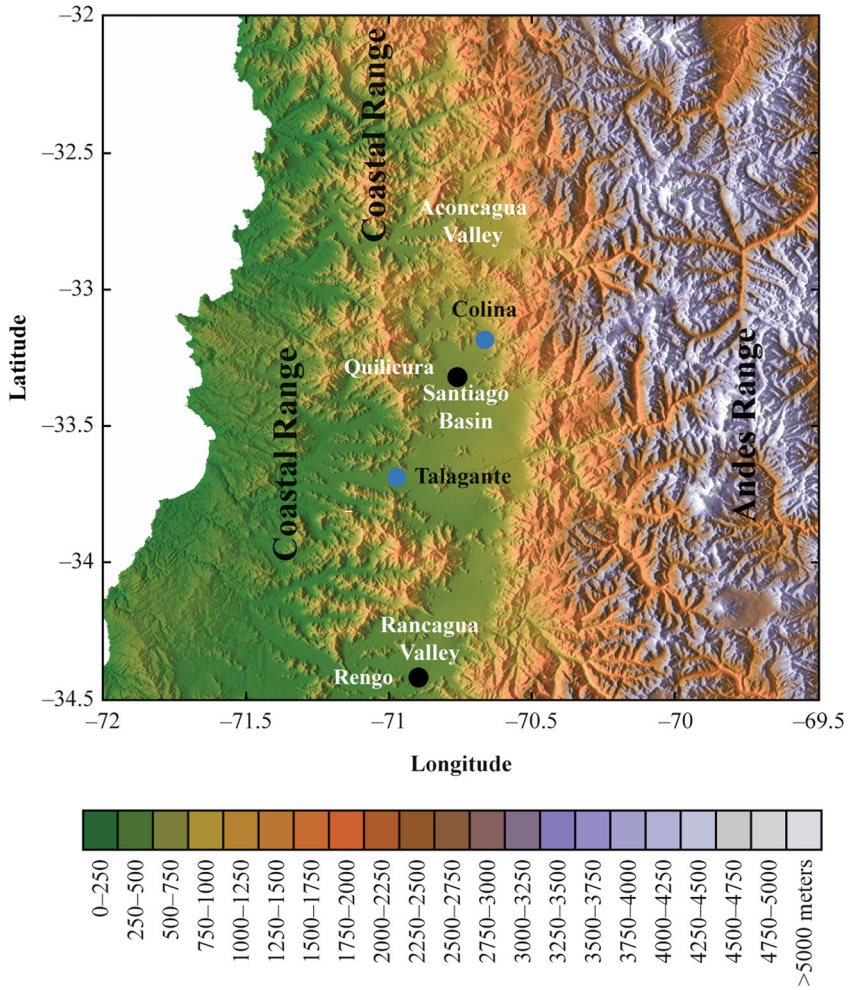

Fig. 1 Geographic features of the study area—blue circles represent the locations of ozonesonde launches

Surface observations at Talagante

Hourly measurements of pollutants (O_3, NO_x, CO) and surface meteorological variables (temperature, water vapor, pressure, wind speed, and wind direction) were monitored continuously during the stratospheric ozone intrusion campaigns to identify other non-stratospheric sources that could enhance surface-level ozone. Nitrogen oxides are useful in identifying the age of plumes and distinguishing local sources from remote ones, due to their shorter lifetime compared to carbon monoxide.

Ozone mixing ratios were determined using a continuous analyzer based on UV absorption technique (Model 49i, Thermoscientific Inc., USA, www.thermoscientific.com). The instrument had a minimum detection limit of 1.0 ppbv, response time of 10 s, and an absolute accuracy of 2%. NO_x levels were determined using a chemiluminescence analyzer (Model 42i, Thermoscientific Inc., USA). NO_2 values were converted to NO using a molybdenum converter heated to nearly 325 °C. The instrument had a minimum detection limit of 1.0 ppbv, response time of 120 s, and an absolute accuracy of 1%. Carbon monoxide levels were determined using continuous monitors based on infrared radiation absorption technique (Model 48i, Thermoscientific Inc. USA,). The analyzer had a minimum detection limit of 40 ppbv, response time of 60 s, and an accuracy of 2%.

Acquisition of ozone data

Two-second average ozone measurements were executed to obtain vertical ozone observations at the Colina and Talagante sites. Ozone profiles were measured using electrochemical concentration cell (ECC) ozonesondes (Model 6A ECC, Science Pump Corporation, USA) carried by 1.2-kg rubber balloons (Totex Corporation, Japan). The ascent rates of the balloons were typically 3–6 m s^{-1} with burst altitudes in the range of 30–35 km. Ground-based 400–406 MHz receivers received the transmitted data at 1-s intervals. The ECC sensor consisted of Teflon cathode and anode chambers containing platinum electrodes immersed in KI solutions of different concentrations (Komhyr 1969). The concentration of the KI solution in the sensor cathode chamber was 1%.

Vertical profiles for meteorological variables (pressure, temperature, and relative humidity (RH)) were recorded using Vaisala RS92-SGP radiosondes. Calibration of the pressure, temperature, and humidity sensors was conducted using Vaisala Ground Check Set GC25. Each sonde's global positioning system (GPS) provided latitude, longitude, altitude, wind speed, and wind direction data.

Analysis from sounding

Tropopause

The boundary between the troposphere and the stratosphere was determined from the temperature profile measurements, in accordance with the World Meteorological Organization (1957) definition of the first and second tropopause (if they exist):

(a) The first tropopause is defined as the lowest level at which the lapse rate decreases to 2 °C/km or less, provided also the average lapse rate between this level and all higher levels within 2 km does not exceed 2 °C/km.
(b) If above the first tropopause the average lapse rate between any level and all higher levels within 1 km exceeds 3 °C/km, then a second tropopause is defined by the same criterion as under (a). This tropopause may be either within or above the 1 km layer.

Ozone within the lower free troposphere

To determine the ozone mixing ratio within the free troposphere, we calculated the ozone distributed from the top of the mixing layer up to the height at which the water vapor mixing ratio (mass of water vapor/dry air mass) decreases below 1 mg/kg. By doing this, we have attempted to minimize the influence of both ozone formed within the mixing layer and ozone of stratospheric origin that retained its low water content.

The top of the CBL was determined from sonde variables such as RH, temperature, and ozone mixing ratio. Normally, sharp decreases in RH and ozone mixing ratio as a function of altitude indicate the top of the CBL while the potential temperature θ remains approximately constant within a well-mixed boundary layer (Nielsen-Gammon et al. 2008).

Total column ozone

Firstly, the total column ozone was estimated by integrating the ozone partial pressure from the surface to the altitude at which the balloons burst. Equation 1, used by the Vaisala DigiCORA sounding system, calculates the result in Dobson units (DU) when ozone partial pressures (p_{O3}) and ambient pressures (p) are represented in millipascals and hectopascals, respectively.

$$\text{Ozone Column} = \sum_i 3.9449 \cdot \left(p_{O_3 i} + p_{O_3 i+1}\right) \ln\left(\frac{p_i}{p_i + 1}\right) \quad (1)$$

where i represents the index for a measurement point.

Secondly, the remaining portion of the ozone column that is not sampled by the ECC was calculated through an extrapolation of the measured ozone profile. This method sums the climatological values to the integrated balloonsonde column to derive total ozone (McPeters et al. 1997). The correction is based on profile measurements from the solar backscattered ultraviolet (SBUV) instrument on the Nimbus 7 satellite.

Figure 2 shows the correlation between satellite products registered by the Aura Ozone Monitoring Instruments (OMI) and the total column ozone computed by adding SBUV climatological amounts. The OMI products selected are based on the Differential Optical Absorption Spectroscopy (DOAS) and the Total Ozone Mapping Spectrometer (TOMS). The better fit was obtained from TOMS-like observations at 1° lat/lon grids ($r^2 = 0.85$). The average differences between corrected ozonesondes and DOAS, TOMS-like (1°), and TOMS-like (0.25°) were 12, 9, and 10 DU respectively. The average error was less than 5% in the three comparisons.

Tropospheric column ozone

The tropospheric column ozone was estimated by integrating the ozone partial pressure from the surface to the first tropopause using Eq. 1.

Results and discussion

Vertical distribution of ozone

A total of 17 ozonesondes were launched from Colina to determine (1) the ozone mixing ratio in the lower free troposphere and (2) tropospheric column ozone. We characterized the stratospheric ozone distribution and its seasonal variability firstly as the tropospheric ozone burden depends in part on the STE.

The total column ozone experienced significant decrease in summer and autumn. Subsequently, the total column recovered during the winter and spring months. Figure 3a shows that from December 2010 to June 2011, the total column ozone reached values as low as 240 DU.

Additionally, vertical ozone profile analysis identified two periods of the year when the tropopause reached the lowest heights. Occasional descent of the tropopause to approximately 11 km occurred during the spring months (Sep–Nov). Subsequently, the tropopause rose above 16 km (Nov–Feb)

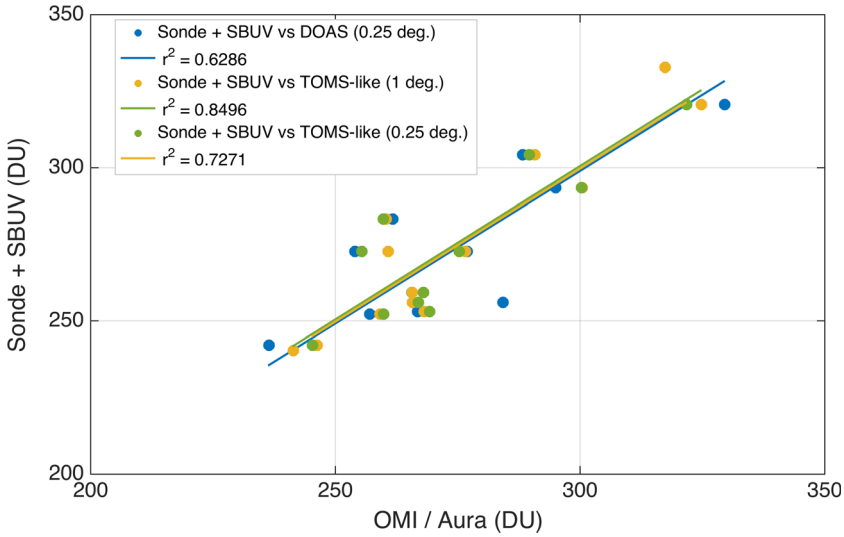

Fig. 2 Ozonesonde total column ozone extrapolated by adding SBUV climatological amounts versus satellite-derived estimates of the total column ozone. Bounding box (OMI products): 72 W, 33 S, 70 W, 32.5 S

and finally descended again to ~ 11 km in the autumn and winter months (Apr–Aug).

Often, the transition between the troposphere and the stratosphere is not that clear as in summer months. In fact, first and second tropopauses were frequently found according to the WMO (1957) definition (Fig. 3b). Double tropopauses exhibit a strong seasonal pattern and often occur in spring, winter, and autumn. On the other hand, the summer months analyzed did not show double tropopauses. A more detailed view of thermal structures shows unstable transitions (Fig. 4). Double tropopauses over central Chile are associated with a characteristic break in the thermal tropopause near the subtropical jet, wherein the tropical tropopause extends to higher latitudes, overlying the lower tropopause (Randel et al. 2007).

Figure 3c illustrates the box plot for ozone in the free troposphere. An increase in the median ozone was observed in the

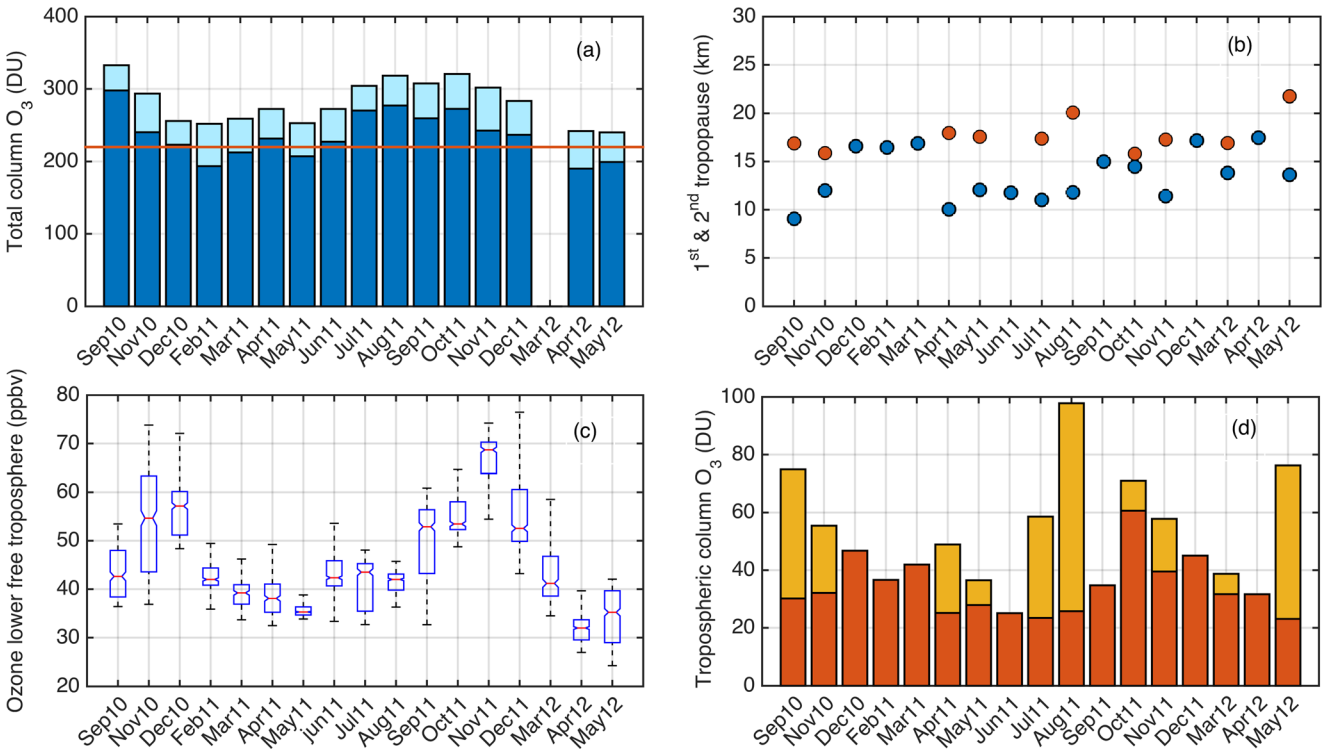

Fig. 3 Ozone variability over central Chile. **a** Total column ozone measured by ozonesonde (blue) and extrapolation computed by adding SBUV climatological amounts (light blue). The red line represents 220 DU, which is conventionally defined as an "ozone hole." **b** Altitude of the first and second tropopause. **c** Ozone mixing ratio in the lower free troposphere. **d** Tropospheric column ozone until the conventional first tropopause (red) and the portion of the column between the first and second tropopause (yellow)

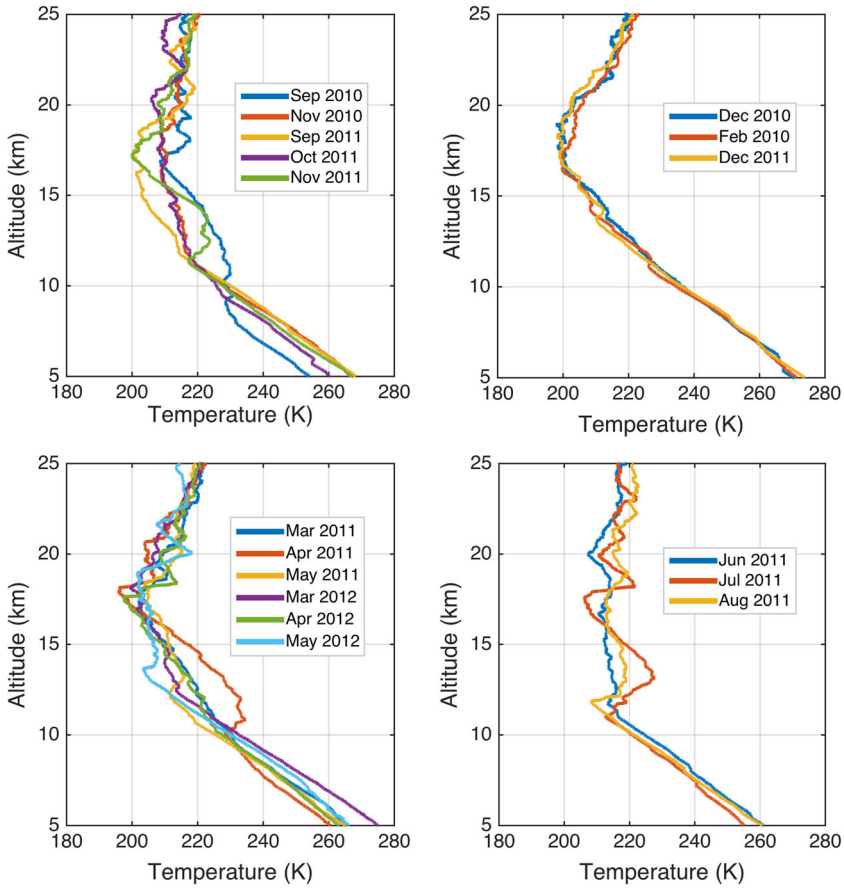

Fig. 4 Temperature profiles over Colina between September 2010 and May 2012

beginning of spring in September 2011. Medians up to 69 ppbv were observed in November 2011. Seasonal maximum in the northern hemisphere occurs during early spring as VOCs accumulated during winter initiate photochemical reactions that lead to ozone peak (Penkett and Brice 1986; Monks 2000). After December 2010, the mixing ratio decreased until it reached minimum values in autumn and winter. Lowest median of 35 ppbv was observed in May 2011.

The variability of tropospheric column ozone, calculated by integrating until the altitude of the fist tropopause, reflects different processes that occur in the troposphere. The most evident variation was decrease in the column to 25 DU between April 2011 and August 2011. This decrease was due to the lower tropopause (11 km) as well as lower photochemical activity during this period (Fig. 3d). Conversely, in the months of December (2010 and 2011) and March (2011), the tropospheric column ozone was higher than 40 DU. This can be attributed to higher tropopause and surface ozone of anthropogenic origin. In October 2011, tropospheric column ozone increased to 61 DU in part due to slightly lower tropopause (14 km) and surface photochemical smog. Additionally, in this case, the ozonesonde indicated that the increase in the tropospheric column ozone was due to STE, which is very common at this time of the year (Fig. S2). Schoeberl (2004) explained that the build-up of tropospheric ozone in spring was caused by mass transfer from the lowermost stratosphere to the troposphere, favored by the movement of the tropopause height upward before summer.

Figure 3d also shows the portion of the column ozone determined between the first and second tropopause. It is worth noticing that the amount within the double tropopause represents a significant quantity with the potential to be transported down into the lower troposphere.

Figure 5 shows the vertical ozone profiles aggregated according to the seasons. In the southern hemisphere, September–November (SON) is considered as spring, December–February (DJF) is considered as summer, March–May (MAM) is considered as autumn, and June–August (JJA) is considered as winter. Figure 5a shows that STE occurred both in spring and winter. However, its contribution to the free troposphere is more significant during spring. In summer and autumn, significant STE was not observed. Finally, Fig. 5b shows that from spring to summer, ozone mixing ratio decreased in the free troposphere but increased in the mixing layer. With respect to the autumn-winter period, the ozone mixing ratio increased in the free troposphere and decreased in the mixing layer from autumn to winter. These variations highlight the influences of the STE and surface photochemistry in the free troposphere.

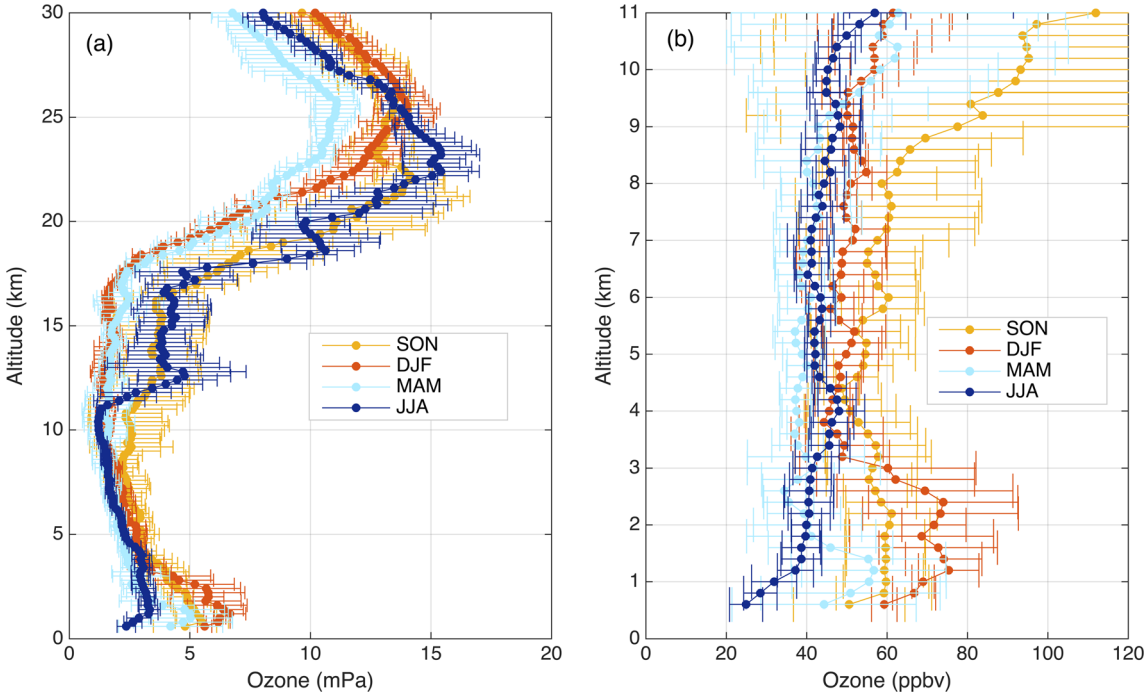

Fig. 5 Ozone vertical profiles in **a** mPa and **b** ppbv aggregated according to meteorological seasons, i.e., September–October (SON), December–February (DJF), March–May (MAM), and June–August (JJA). The bars represent the standard deviation of each group

To conclude this section, we compared our data with ozonesonde values obtained from the Easter Island, located in front of central Chile, in a region subject to intrusions and double tropopauses. Tropospheric column ozone median (32 DU) in central Chile is 5 DU higher than the annual median measured in the Easter Island, where the typical values range between 10 and 45 DU (Gallardo et al. 2016). The lower minimum values found in the island compared to those of central Chile can be explained by the photochemical activity driven through anthropogenic precursors present in the mixing layer of central Chile (Fig. 5b). In Easter Island, spring maxima in tropospheric column ozone have also been reported.

Case studies

Two case studies are presented to illustrate the process of STE and its impact on the vertical distribution of O_3, and surface O_3. Both cases involved fronts crossing central Chile as during these events it is more likely the occurrence of STE. For instance, in Cerro Tololo (2.2 km asl), located to the north of the Santiago basin, Rondanelli et al. (2002) explained the surface ozone variability during winter and early spring as a consequence of deep troughs and cutoff low systems energetic enough to transport stratospheric ozone-rich air from polar latitudes.

Furthermore, as discussed in "Vertical distribution of ozone," September is of significant interest because (1) the total column ozone attains high values during the seasonal cycle, and (2) the tropopause is relatively low in altitude and therefore, greater STE is expected. Once the stratospheric air from a tropopause fold has been irreversibly transported into the troposphere, it will eventually become well mixed within the troposphere (Cooper et al. 2004).

The second period selected was in March due to its significant contrast with September. In March, the total column ozone reached minimum values within the seasonal cycle, and the tropopause was at relatively higher altitude. Consequently, STE was expected to be less significant.

Frontal system: late winter case study (September 1–5, 2014)

Ozonesondes were launched during the passage of a characteristic winter frontal system. The system arrived in the Santiago basin on the morning of September 1, 2014, and passed completely by the afternoon of September 5, 2014. To describe the front, we have performed the reanalysis of the geopotential height at 500 hPa pressure level, zonal wind, and omega (vertical velocity) at 6 UTC (03:00 local time) during the same days of the ozonesonde launches (Kalnay et al. 1996). The evolution of the geopotential height (Fig. 6) depicts a strong low passing over the southwestern part of South America. The zonal wind above 33° S (pressure versus longitude) shows higher values between ~200 and 400 hPa (> 30 m/s) for September 1 and September 3. Also, Fig. 6 shows the portions of the atmosphere where descent motions are more likely to occur (omega > 0.1 Pa/s).

Figure 7a shows the vertical ozone profile for September 3, 2014, and September 5, 2014, at 12:00 (local time). The

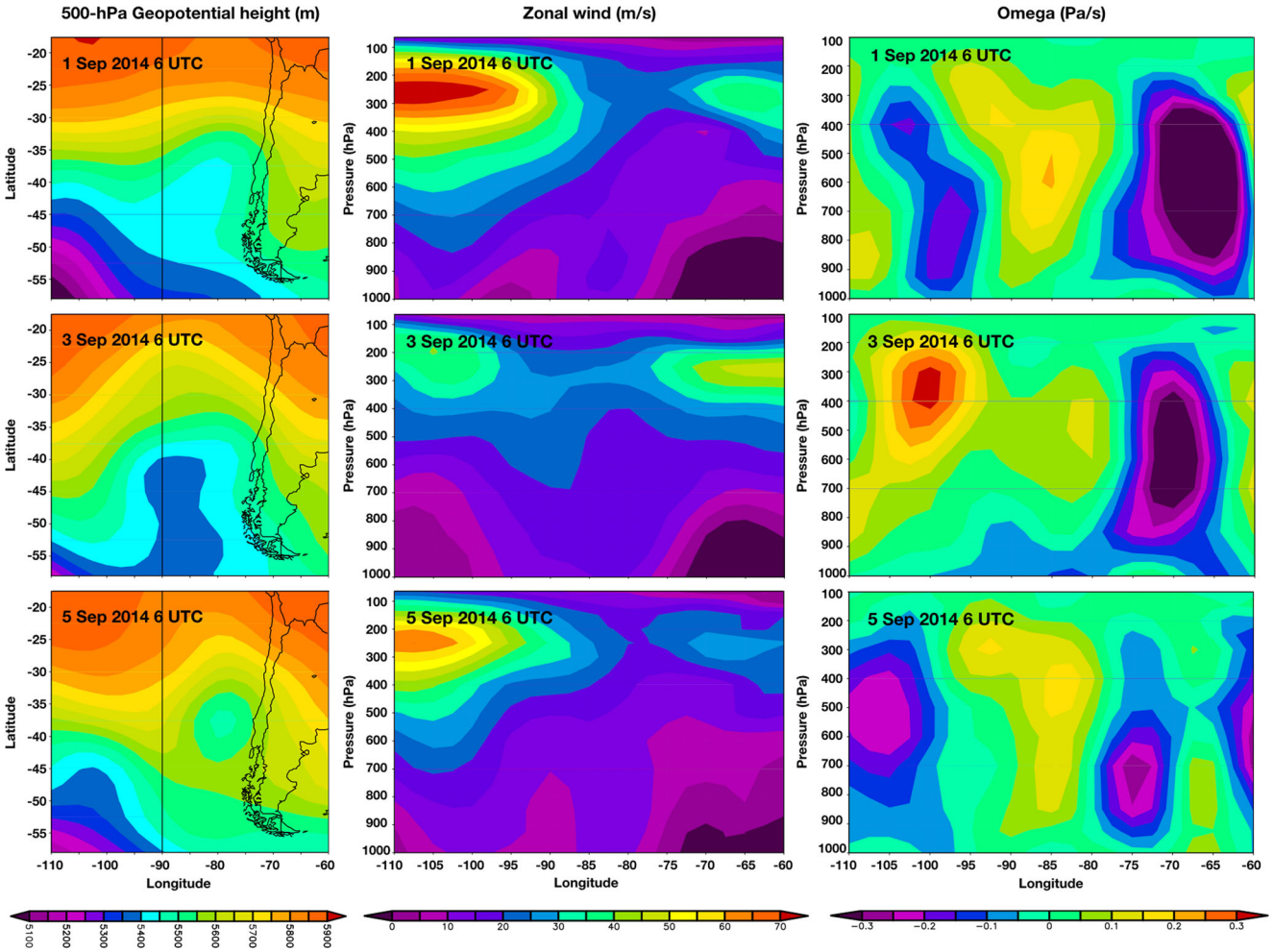

Fig. 6 Five hundred-hectopascal geopotential height (left panel). Cross-section of the zonal wind over 33° S (middle panel), and cross section of omega over 33° S (right panel) at 6 UTC (03:00 local time) during the same days of the ozonesonde launches (frontal system). Data: 6 hourly NCEP/NCAR reanalysis

tropopause on September 3 was located at 10.0 km and had dropped slightly by 0.1 km compared to September 1 (Fig. 7c). On September 5, significant ozone intrusion was observed up to ~ 6 km. Additionally, the descent of stratospheric air had significant effect on the tropopause calculation, which decreased to 7.3 km. The lapse rate behind the cold front is especially colder between 3.0 and 7.3 km compared to prior days. Figure 7b also shows the drastic decrease in water vapor mixing ratio on September 5. Low water content detected in the atmosphere over 3 km is a strong indicator of the stratospheric influence on the free troposphere. Besides, the potential temperature calculated from the radiosondes indicates a marked difference in the atmosphere above and below ~ 3 km on September 5 (Fig. 7d).

The stratospheric ozone intrusion detected on September 5 increased the tropospheric column ozone by 9 DU, which represents a rapid and significant increase of 44%. For this calculation, the initial height of the tropopause (10 km) was used to avoid distortion in the tropopause calculation caused by the intrusion of stratospheric air (Table 1).

Surface ozone observations (frontal system)

As highlighted in Fig. 8, ozone at the surface level increased steadily from the morning of September 4, and attained the highest MDA8 (maximum daily 8-h average) of 40 ppbv on September 7. Analysis of the vertical profiles and mixing ratios of carbon monoxide and nitrogen oxides indicates that ozone increase may be attributed to two different processes: stratospheric transport and photochemical production.

An increase in the ozone mixing ratio between the morning of September 4 and September 5 occurred in a period without significant photochemical precursors. Concurrently, carbon monoxide levels reached the lowest values of the week (~ 1 parts per million volume (ppmv)). For other days of the week, carbon monoxide exhibited typical spikes, probably due to residential combustion and mobile sources. In addition, on the morning of

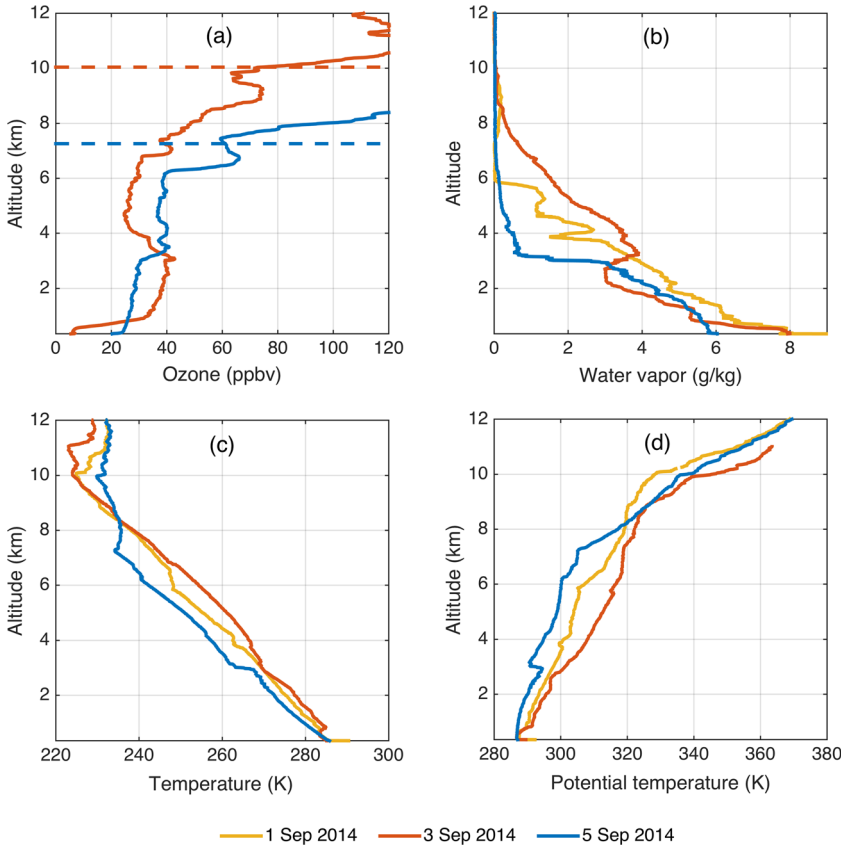

Fig. 7 **a** Vertical ozone, **b** water vapor mixing ratio, **c** temperature, and **d** potential temperature profiles for launches on September 1, 2014, September 3, 2014, and September 5, 2014, over Talagante at 12:00 local time. Dashed lines indicate tropopause heights

September 4 and night of September 5, primary emissions of nitric oxide dropped to less than 5 ppbv. Therefore, ozone titration by nitric oxide did not occur. Moreover, nitrogen dioxide mixing ratios were also lower (< 7 ppbv) and could not have led to enough ozone formation by local photochemical processes. The MDA8 for ozone was 25 ppbv on September 5, which was higher than the values of the preceding days (12, 5, 8, and 18 ppbv on September 1, 2, 3, and 4, respectively).

Further, additional evidence to support possible stratospheric influence on surface ozone levels was presented by unusually enhanced ozone mixing ratio observed during nighttime from midnight on September 4 to dawn on September 5. During this period, westerly winds precluded possible ozone transport from Santiago City, while photochemical production was overruled as it occurs only during daytime. Besides, as shown in Fig. 6, the values of omega suggest that descent motion is occurring. The nightly ozone average (19:00–06:00 local time) was 10 ppbv higher than the monthly nighttime average (8.5 ppbv), as determined for the months of September 2010–2014 at Talagante. Similar nighttime patterns were also detected by Santiago's official monitoring network extending at least 140 km north and south of Talagante, indicating large-scale transport from the westerly direction. Nighttime maxima for the north (Quilicura) and south (Rengo) locations corresponded to 18 and 22 ppbv, respectively (Fig. 9).

Table 1 Tropospheric column ozone (TCO) and variations in the tropopause measured at the beginning of the events

Date	Initial tropopause (km)	TCO below the initial tropopause (DU)	TCO variation (%)
Sep. 3, 2014	10.0	20.22	–
Sep. 5, 2014	–	29.17	44 (Sep. 5–Sep. 3)
Mar. 23, 2015	12.4	19.55	–
Mar. 24, 2015	–	24.89	27 (Mar. 24–Mar. 23)
Mar. 26, 2015	–	23.10	–
Mar. 27, 2015	–	28.94	48 (Mar. 27–Mar. 23)

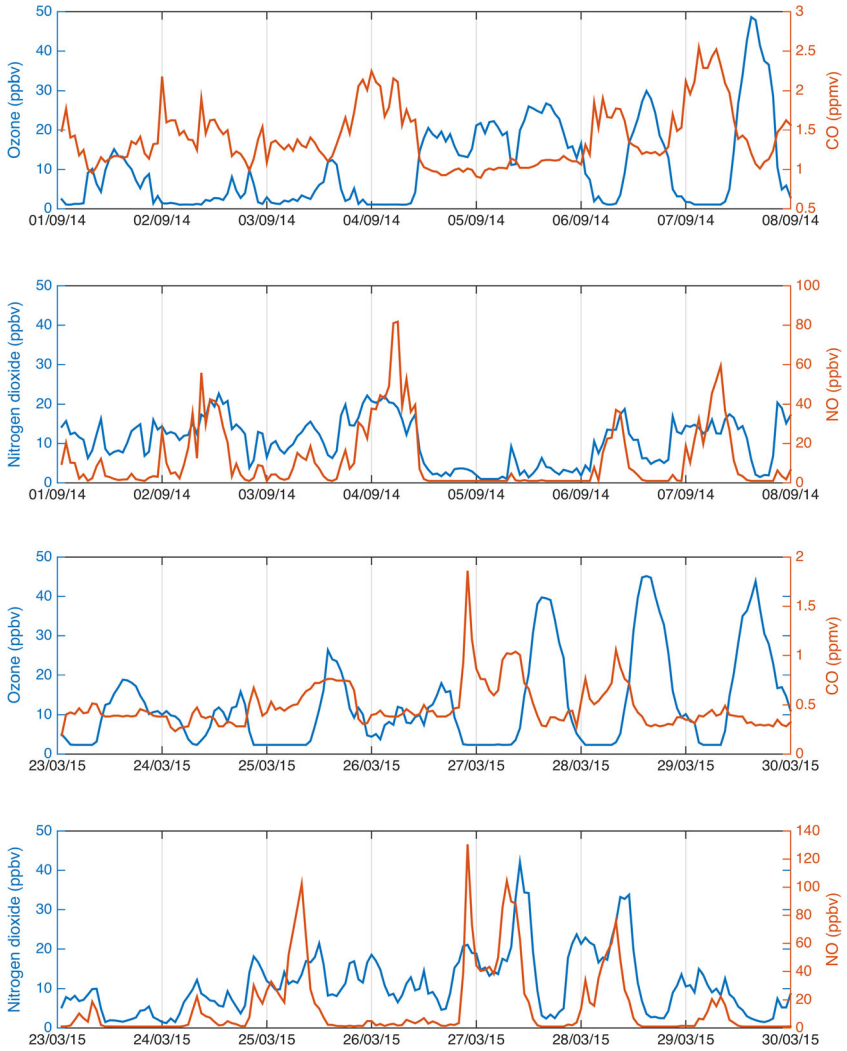

Fig. 8 Surface-level diurnal variations of ozone, carbon monoxide, nitrogen dioxide, and nitric oxide at Talagante during the frontal system and cutoff low

Conversely, for the weekend, photochemical production of ozone was more likely. Higher nitric oxide and carbon monoxide mixing ratios in the morning with high nitrogen dioxide mixing ratios until photolysis led to ozone

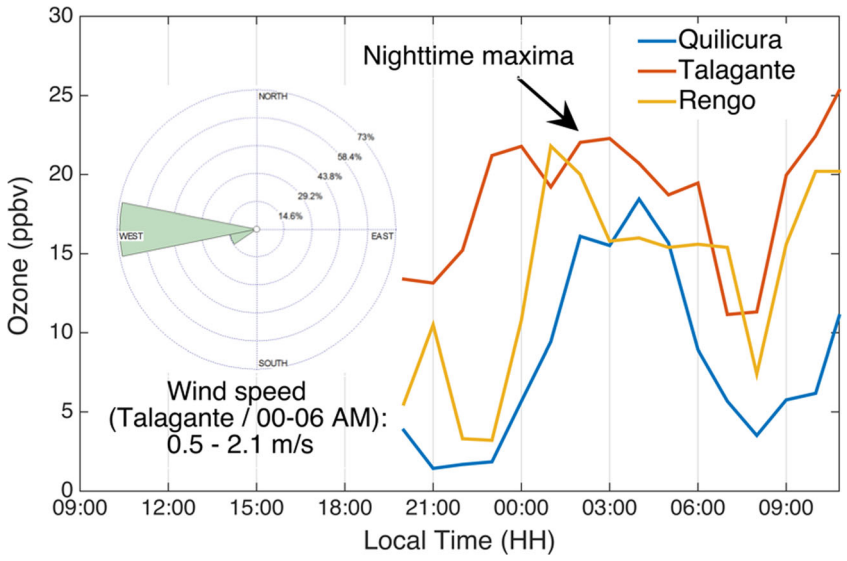

Fig. 9 Ozone nighttime maxima and wind speed between 00:00 and 06:00 at Talagante in central Chile

accumulation few hours after noon when the mixing layer was fully developed.

Cutoff low: early autumn case study (March 23–27, 2015)

Ozonesondes were launched during the passage of a cutoff low, which commonly occurs during non-winter periods. The cutoff low arrived in the Santiago basin on the morning of March 23, 2015, and migrated midday on March 27, 2015, after causing heavy rains. Figure 10 shows the reanalysis of the geopotential height at 500 hPa pressure level, zonal wind, and omega at 6 UTC (03:00 local time) during the same days of the ozonesonde launches. The geopotential height on March 24 shows a closed low near 33° S, 78° W approaching to the continent. Above central Chile, strong descent conditions (omega > 0.1 Pa/s) were observed over the last day of precipitations (September 27). For more details of this particular meteorological event, refer to Barrett et al. (2016).

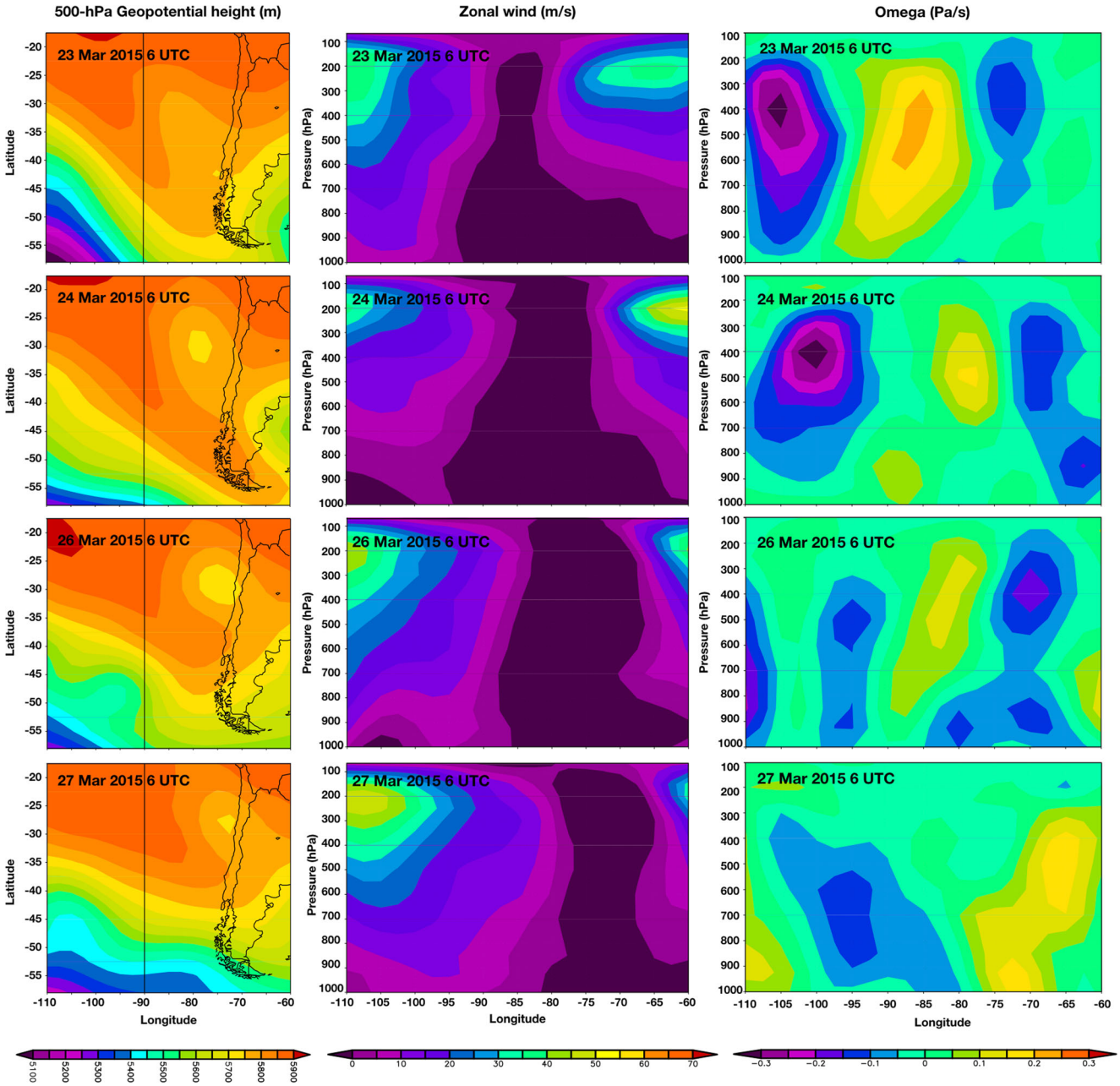

Fig. 10 Five hundred-hectopascal geopotential height (left panel). Cross section of the zonal wind over 33° S (middle panel) and cross section of omega over 33° S (right panel) at 6 UTC (03:00 local time) during the same days of the ozonesonde launches (cutoff low). Data: 6 hourly NCEP/NCAR reanalysis

Figure 11 illustrates the results of the ozonesondes conducted on March 23, 24, 26, and 27, 2015. The tropopause was located at 12.4, 12.4, 11.4, and 12.6 km, respectively (Fig. 11a). The first evidence of an intrusion was observed on March 24. However, the ozone increase was limited to the upper troposphere. Figure 11c shows the increase of the ozone mixing ratio up to ~ 10 km. Consistently, Fig. 11e reveals very dry atmosphere above 10 km. In contrast, the tropospheric column ozone increased by 5 DU compared to the previous day, representing 27% increase (Table 1).

Comparison between the final days of the episode (March 26 and 27, 2015) showed considerable ozone increase in the free troposphere (Fig. 11d). Additionally, significant decrease in the water content from ~ 4 km in altitude was noted (Fig. 11f). Further, the tropospheric column ozone at the end of the cutoff low was 29 DU. This represented 25% increase from the previous day, and total increase of 48% from the beginning of the cutoff low (Table 1).

Surface ozone observations (cutoff low)

At the surface level, rapid ozone increase occurred after the cutoff low passed through the Santiago basin (Fig. 8). The observed ozone formation can be explained by the availability of ozone precursors. For instance, on the morning of March 27, 2015, higher NO_2 mixing ratios (as high as 42 ppbv), compared to previous days can explain ozone formation later in the afternoon when the daily maximum reached 40 ppbv. Likewise, low wind speed (< 1 m s^{-1}) favored local ozone formation and can explain the high

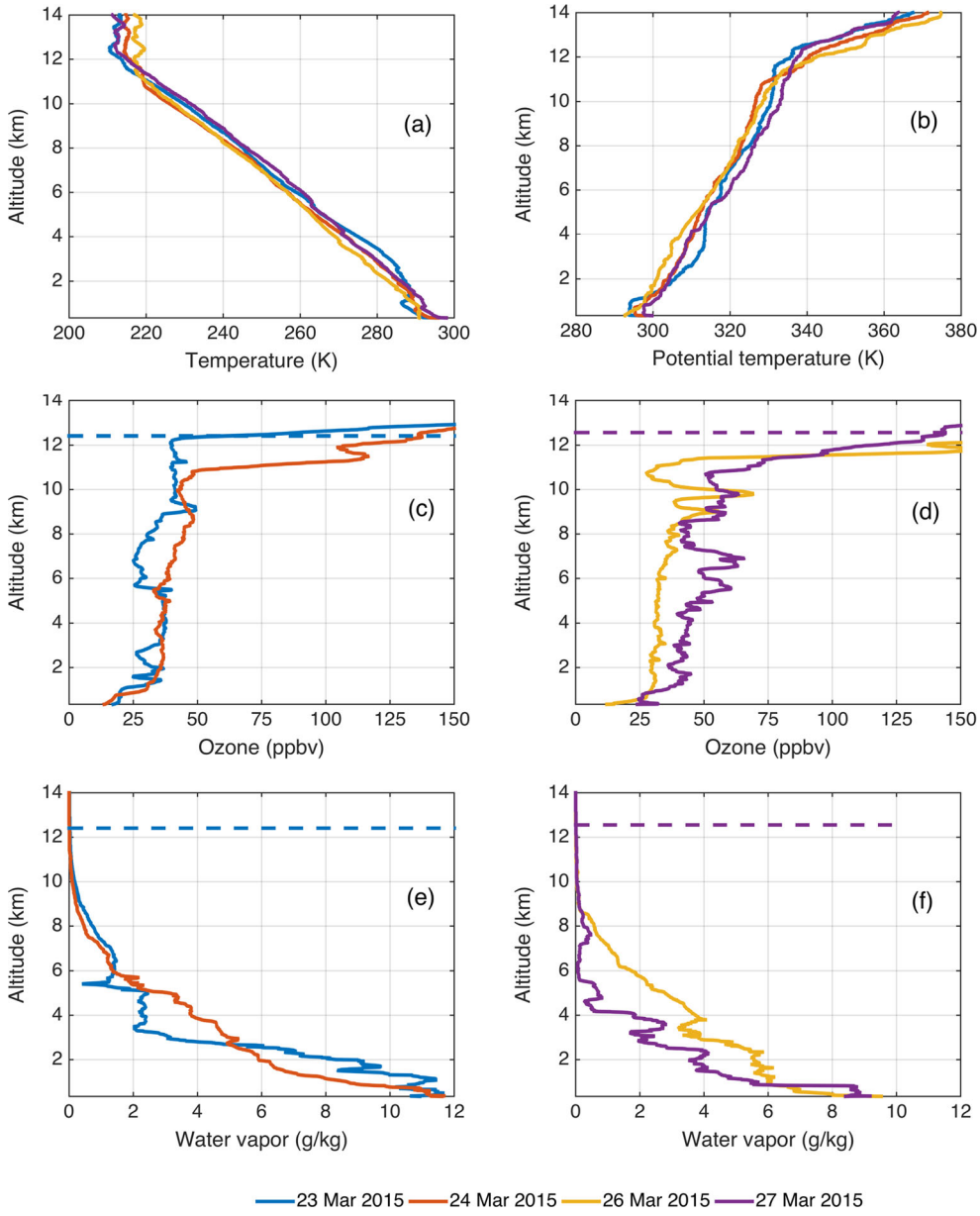

Fig. 11 Vertical profiles over Talagante at 12:00 local time. **a** Temperature profiles on March 23, 2015, March 24, 2015, March 26, 2015, and March 27, 2015. **b** Potential temperature profiles on March 23, 2015, March 24, 2015, March 26, 2015, and March 27, 2015. **c** Ozone profiles on March 23, 2015 and March 24, 2015. **d** Ozone profiles on March 26, 2015 and March 27, 2015. **e** Water vapor mixing ratio on March 23, 2015 and March 24, 2015. **f** Water vapor mixing ratio on March 26, 2015 and March 27, 2015. Dashed lines indicate tropopause heights in all panels

comparability between nitrogen dioxide and ozone mixing ratios. During that day, the influence from the lower troposphere appeared insignificant. Although, for the following days, especially on March 29, 2015, contribution from the layers above became more likely as measured mixing ratios of nitrogen oxides were smaller, and carbon monoxide decreased to values as low as 0.3 ppmv. In addition, the vertical analysis of March 27, 2015, showed significant amounts of ozone available to be entrained into the CBL.

Conclusions

The tropospheric column ozone at central Chile falls within the range of 23–61 DU. Columns aggregated by seasons exhibited significant differences between summer and winter: December–February (43 ± 5 DU), March–May (30 ± 7 DU), June–August (25 ± 1 DU), and September–October (39 ± 12 DU).

Higher tropopause and surface ozone produced by photochemical reactions involving precursors from anthropogenic sources contributed to tropospheric column ozone build-up during the summer. In spring, larger STE explained the increase of ozone in the upper troposphere.

The incidents of stratospheric intrusions analyzed during late winter and early fall were accompanied by significant and fast ozone increases in the free troposphere. This downward transport was traced to as low as 3 km above the sea level behind the winter front. The tropospheric column ozone increases 44% (September) and 48% (March) behind the cold fronts.

Surface ozone enhancement detected over a large area of central Chile during nighttime of September 4–5, 2014, cannot be explained by local photochemical production. Instead, we suggest the downward motion of ozone-rich air detected above 3 km as the low-pressure system passed, as the more likely explanation.

Funding This work has been funded by the FONDECYT Program, initiation into research 2013, Project No. 11130177.

References

Alvim DS et al (2017) Main ozone-forming VOCs in the city of Sao Paulo: observations, modelling and impacts. Air Qual Atmos Health 10:421–435. https://doi.org/10.1007/s11869-016-0429-9

Anet JG, Steinbacher M, Gallardo L, Velásquez Álvarez PA, Emmenegger L, Buchmann B (2017) Surface ozone in the southern hemisphere: 20 years of data from a site with a unique setting in El Tololo, Chile. Atmos Chem Phys 17:6477–6492. https://doi.org/10.5194/acp-17-6477-2017

Barrett BS, Campos DA, Veloso JV, Rondanelli R (2016) Extreme temperature and precipitation events in March 2015 in central and northern Chile. J Geophys Res: Atmos 121:4563–4580. https://doi.org/10.1002/2016JD024835

Bell ML, McDermott A, Zeger SL, Samet JM, Dominici F (2004) Ozone and short-term mortality in 95 US urban communities, 1987-2000. JAMA 292:2372–2378. https://doi.org/10.1001/jama.292.19.2372

Cooper O et al (2004) On the life cycle of a stratospheric intrusion and its dispersion into polluted warm conveyor belts. J Geophys Res: Atmos 109. https://doi.org/10.1029/2003JD004006

Danielsen EF (1968) Stratospheric-tropospheric exchange based on radioactivity, ozone and potential vorticity. J Atmos Sci 25:502–518

Fiore AM, Naik V, Leibensperger EM (2015) Air quality and climate connections. J Air Waste Manage Assoc 65:645–685. https://doi.org/10.1080/10962247.2015.1040526

Gallardo L, Henríquez A, Thompson AM, Rondanelli R, Carrasco J, Orfanoz-Cheuquelaf A, Velásquez P (2016) The first twenty years (1994–2014) of ozone soundings from Rapa Nui (27°S, 109°W, 51 m a.s.l.) Tellus B Chem Phys Meteorol 68:29484. https://doi.org/10.3402/tellusb.v68.29484

Hegglin MI, Shepherd TG (2009) Large climate-induced changes in ultraviolet index and stratosphere-to-troposphere ozone flux. Nat Geosci 2:687–691 http://www.nature.com/ngeo/journal/v2/n10/suppinfo/ngeo604_S1.html

Kalnay E et al (1996) The NCEP/NCAR 40-year reanalysis project. Bull Am Meteorol Soc 77:437–471. https://doi.org/10.1175/1520-0477(1996)077<0437:tnyrp>2.0.co;2

Komhyr WD (1969) Electrochemical cells for gas analysis. Ann Geophys 25:203–210

Lee DS, Holland MR, Falla N (1996) The potential impact of ozone on materials in the U.K. Atmos Environ 30:1053–1065. https://doi.org/10.1016/1352-2310(95)00407-6

Lippmann M (1991) Health effects of tropospheric ozone. Environ Sci Technol 25:1954–1962. https://doi.org/10.1021/es00024a001

Liu JC, Peng RD (2018) Health effect of mixtures of ozone, nitrogen dioxide, and fine particulates in 85 US counties. Air Qual Atmos Health. https://doi.org/10.1007/s11869-017-0544-2

McConnell R et al (2002) Asthma in exercising children exposed to ozone: a cohort study. Lancet 359:386–391. https://doi.org/10.1016/s0140-6736(02)07597-9

McPeters RD, Labow GJ, Johnson BJ (1997) A satellite-derived ozone climatology for balloonsonde estimation of total column ozone. J Geophys Res: Atmos 102:8875–8885. https://doi.org/10.1029/96JD02977

Monks PS (2000) A review of the observations and origins of the spring ozone maximum. Atmos Environ 34:3545–3561. https://doi.org/10.1016/S1352-2310(00)00129-1

Monks PS et al (2015) Tropospheric ozone and its precursors from the urban to the global scale from air quality to short-lived climate forcer. Atmos Chem Phys 15:8889–8973. https://doi.org/10.5194/acp-15-8889-2015

National Research Council, Committee on C, Physics of Ozone D (1982) Causes and effects of stratospheric ozone reduction, an update: a report / prepared by the Committee on Chemistry and Physics of Ozone Depletion and the Committee on Biological Effects of Increased Solar Ultraviolet Radiation, Environmental Studies Board, Commission on Natural Resources, National Research Council. vol Accessed from http://nla.gov.au/nla.cat-vn302643. National Academy Press, Washington, D.C

Neuman JA et al (2012) Observations of ozone transport from the free troposphere to the Los Angeles basin. J Geophys Res: Atmos 117. https://doi.org/10.1029/2011jd016919

Nielsen-Gammon JW et al (2008) Multisensor estimation of mixing heights over a coastal city. J Appl Meteorol Climatol 47:27–43. https://doi.org/10.1175/2007jamc1503.1

Penkett SA, Brice KA (1986) The spring maximum in photo-oxidants in the northern hemisphere troposphere. Nature 319:655–657

Price JD, Vaughan G (1993) The potential for stratosphere-troposphere exchange in cut-off-low systems. Q J R Meteorol Soc 119:343–365. https://doi.org/10.1002/qj.49711951007

Randel WJ, Seidel DJ, Pan LL (2007) Observational characteristics of double tropopauses. J Geophys Res: Atmos 112. https://doi.org/10.1029/2006JD007904

Roelofs G-J, Lelieveld JOS (1997) Model study of the influence of cross-tropopause O3 transports on tropospheric O3 levels. Tellus B 49:38–55. https://doi.org/10.1034/j.1600-0889.49.issue1.3.x

Rondanelli R, Gallardo L, Garreaud RD (2002) Rapid changes in ozone mixing ratios at Cerro Tololo (30°10′S, 70°48′W, 2200 m) in connection with cutoff lows and deep troughs. J Geophys Res: Atmos 107:4677. https://doi.org/10.1029/2001JD001334

Schoeberl MR (2004) Extratropical stratosphere-troposphere mass exchange. J Geophys Res: Atmos 109. https://doi.org/10.1029/2004JD004525

Schultz MG et al (2017) Tropospheric ozone assessment report: database and metrics data of global surface ozone observations. Elem Sci Anth 5:58. https://doi.org/10.1525/elementa.244

Seguel RJ, Morales SR, Leiva GM (2012) Ozone weekend effect in Santiago, Chile. Environ Pollut 162:72–79. https://doi.org/10.1016/j.envpol.2011.10.019

Seguel RJ, Mancilla CA, Rondanelli R, Leiva MA, Morales RGE (2013) Ozone distribution in the lower troposphere over complex terrain in Central Chile. J Geophys Res: Atmos 118:2966–2980. https://doi.org/10.1002/jgrd.50293

Staehelin J, Mäder J, Weiss AK, Appenzeller C (2002) Long-term ozone trends in northern mid-latitudes with special emphasis on the contribution of changes in dynamics. Phys Chem Earth A/B/C 27:461–469. https://doi.org/10.1016/S1474-7065(02)00027-X

Stevenson DS et al (2006) Multimodel ensemble simulations of present-day and near-future tropospheric ozone. J Geophys Res: Atmos 111. https://doi.org/10.1029/2005JD006338

Stohl A et al (2000) The influence of stratospheric intrusions on alpine ozone concentrations. Atmos Environ 34:1323–1354. https://doi.org/10.1016/S1352-2310(99)00320-9

Thompson AM et al (2012) Southern Hemisphere Additional Ozonesondes (SHADOZ) ozone climatology (2005–2009): Tropospheric and tropical tropopause layer (TTL) profiles with comparisons to OMI-based ozone products. J Geophys Res: Atmos 117. https://doi.org/10.1029/2011JD016911

Toro R, Donoso C, Seguel RJ, Morales RES, Leiva MG (2013) Photochemical ozone pollution in the Valparaiso Region, Chile. Air Qual Atmos Health:1–11. https://doi.org/10.1007/s11869-013-0218-7

Toro R, Seguel RJ, Morales SRE, Leiva GM (2014) Ozone, nitrogen oxides, and volatile organic compounds in a central zone of Chile. Air Qual Atmos Health:1–13. https://doi.org/10.1007/s11869-014-0306-3

Van Dingenen R, Dentener FJ, Raes F, Krol MC, Emberson L, Cofala J (2009) The global impact of ozone on agricultural crop yields under current and future air quality legislation. Atmos Environ 43:604–618. https://doi.org/10.1016/j.atmosenv.2008.10.033

World Meteorological Organization (1957) Meteorology—a three-dimensional science: second session of the Commission for Aerology. WMO Bull IV(4):134–138

Young PJ et al (2013) Pre-industrial to end 21st century projections of tropospheric ozone from the atmospheric chemistry and climate model intercomparison project (ACCMIP). Atmos Chem Phys 13:2063–2090. https://doi.org/10.5194/acp-13-2063-2013